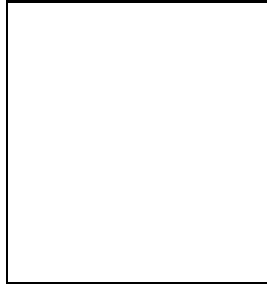


OPEN AND HIDDEN CHARM PRODUCTION WITH THE HERA-B EXPERIMENT

A. BOGATYREV

Institute of Theoretical and Experimental Physics, 117259 Moscow, Russia



Measurements of the suppression of the yield per nucleon and differential distributions of J/ψ production for 920 GeV/c protons incident on heavy nuclear targets have been made with broad coverage in p_T and negative coverage in x_F of produced meson. Production ratios of $\psi(2S)$ to J/ψ and χ_c to J/ψ have been measured with a high accuracy. The D^+ and D^0 production cross sections as well as D^+ to D^0 ratio have been obtained on one of the highest statistics available in proton nucleus experiments.

1 Introduction

The mechanisms by which charmonium and open charm states are produced in hadronic collisions are not well understood and are the focus of much interest. Although most of the results from previous experiments are qualitatively described by different theoretical models, there are some quantitative discrepancies that may be resolved with a better understanding of non-perturbative effects in the production of heavy quarks. Taking into account that the production mechanisms can be identified by their strong kinematic dependences, it is crucial to have new measurements with high statistics and broad kinematic coverage to accomplish comprehensive descriptions of charm production in nuclei. In this context the HERA-B experiment provides new data on open and hidden charm production.

2 The HERA-B Experiment

HERA-B is a fixed target experiment at the HERA storage ring at DESY. Diverse hidden and open charm states are produced in proton-nucleus inelastic collisions. The pN energy in the center of mass corresponds to 41.6 GeV.

The spectrometer emphasizes vertexing, tracking, particle identification and features a dedicated multilevel J/ψ trigger.

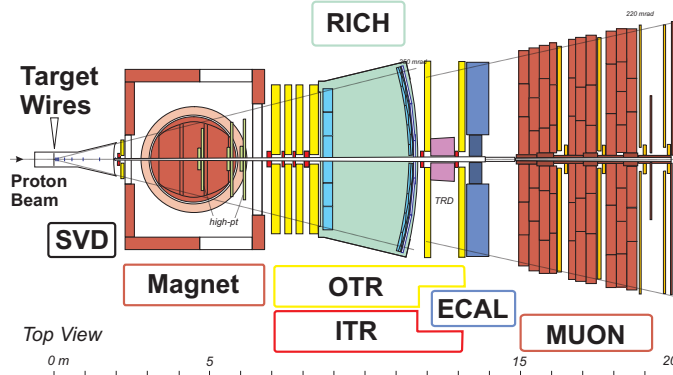


Figure 1: Layout of the HERA-B detector.

The HERA-B target is a fixed target system consisting of two stations separated by 4 cm along the beam direction. Each station houses 4 target wires which can be moved independently into the beam halo.

The side view of the detector is shown in Fig. 1. The protons come from the left and interact in the target region. The target station is followed by the Vertex Detector System(VDS), which provides a precise reconstruction of primary and secondary vertices. The main tracking system(ITR+OTR) is placed behind the VDS. It uses different technologies, depending on the distance to the beam center.

Particle identification is performed by a Ring Imaging Cherenkov Counter(RICH), an Electromagnetic Calorimeter(ECAL) and a MUON detector(MUON).

The J/ψ trigger¹ is initiated by di-lepton signatures from either MUON or ECAL systems. The information on regions of interest defined by pretriggers is used as seeds for the following search for tracks in the tracking system. Then the trigger performs the extrapolation of found tracks through the magnet and follows them through the VDS. In addition a vertex constraint is applied. Events with at least two fully reconstructed di-lepton candidates which come from a common vertex pass the trigger requirements.

3 Data Set 2002/3

The HERA-B collaboration collected data during 3 month data-taking period in 2002/2003. The data samples were obtained using carbon, titanium and tungsten wires. During that time 150 million di-lepton triggered events were acquired. About 170,000 of J/ψ were reconstructed in muon channel and about 150,000 of J/ψ were found in electron channel. The trigger performance has been significantly improved since the year 2000. For comparison, in 2000 the J/ψ rate was 25-35 per hour and in 2002/2003 we already had 1000-1500 J/ψ per hour. Significant improvements in the data acquisition system had been made as well, which resulted in achieving high recording rates, which in turn allowed accumulation of 210 million minimum bias events in just one week of running. The Minimum Bias trigger selected events satisfying a requirement on either a minimum number of hits in RICH or a minimum energy deposited in ECAL. It allowed to suppress events with no interaction without introducing any significant bias.

4 Preliminary results. The Minimum Bias Data

The following open charm decays are fully reconstructed in minimum bias data:

$$D^0 \rightarrow K^- \pi^+$$

$$D^+ \rightarrow K^- \pi^+ \pi^+$$

$$D^{*+} \rightarrow D^0 \pi^+ \quad D^0 \rightarrow K^- \pi^+$$

Throughout this paper charge conjugate decays are also implied.

The invariant mass plots for D^+ and D^0 are shown in Fig. 2 and Fig. 3 respectively. The bump seen to the left of the D^0 in Fig. 3 is produced by reflection of not fully reconstructed charm decays, for instance $D^0 \rightarrow K^- \pi^+ \pi^0$. The shape of this reflection was obtained from MC generated $c\bar{c}$ events and was used in the fit as a component of the background in $K\pi$ invariant mass plot.

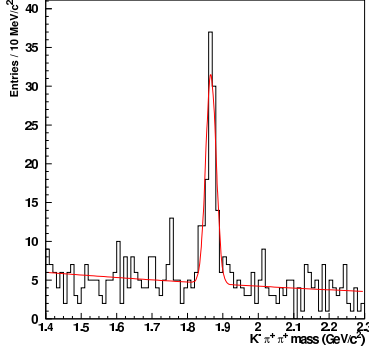


Figure 2: $M(K\pi\pi)$.

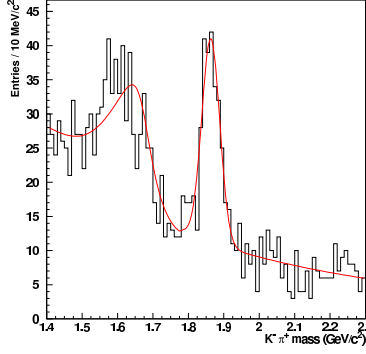


Figure 3: $M(K\pi)$.

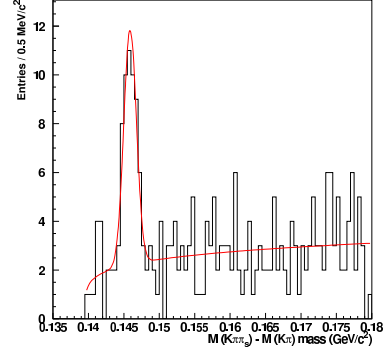


Figure 4: $M(K\pi\pi_{slow}) - M(K\pi)$.

The mass difference between the mass of D^{*+} and the mass of D^0 is shown in Fig. 4. This quantity peaks close to the pion mass and has a very small width. The peak is narrow due to the fact that the errors in calculation of the invariant mass of three particles (in case of D^{*+}) and two particles (in case of D^0) are highly correlated, and therefore cancel out to a large extent.

The signal yields for the fully reconstructed D^+ , D^0 and D^{*+} decays are shown in Table 1.

Table 1: Signal yields for D^0 , D^+ and D^{*+} .

$D^+ \rightarrow K^- \pi^+ \pi^+$	$D^0 \rightarrow K^- \pi^+$	$D^{*+} \rightarrow D^0 \pi^+$
98 ± 12	189 ± 20	43 ± 8

The sample of open charm collected by HERA-B constitutes one of the highest statistics available in proton beam experiments. Therefore the HERA-B will provide the precise measurement of D^0 , D^+ and D^{*+} cross sections as well as $\frac{D^+}{D^0}$ and $\frac{D^{*+}}{D^0}$ ratios.

Table 2: Results on D^+ and D^0 production cross sections.

	$-0.1 < x_F < 0.05$	full x_F
$\sigma(D^+) \mu b / \text{nucl}$	$11.5 \pm 1.7_{\text{stat}} \pm 2.2_{\text{sys}}$	$30.2 \pm 4.5_{\text{stat}} \pm 5.8_{\text{sys}}$
$\sigma(D^0) \mu b / \text{nucl}$	$21.4 \pm 3.2_{\text{stat}} \pm 3.6_{\text{sys}}$	$56.3 \pm 8.5_{\text{stat}} \pm 9.5_{\text{sys}}$

The preliminary results on D^+ and D^0 cross sections are summarized in Table 2. The x_F range of this analysis extends from -0.1 to 0.05. Also shown are the total cross sections which were calculated by extrapolating over the full x_F range. In the calculation of the ratio between D^+ and D^0 cross sections the systematic errors related to detector efficiencies are minimized and the dependence on the absolute luminosity determination is removed. This allows the accurate measurement of the cross section ratio. Result for the $\frac{D^+}{D^0}$ ratio is $0.54 \pm 0.11_{\text{stat}} \pm 0.14_{\text{sys}}$.

The comparison of our measurement for $\frac{D^+}{D^0}$ ratio with those of other experiments is shown in Fig. 5. For the ratio the experimental situation is unclear, and the uncertainties are large

particularly for proton beam experiments. The line on the plot shows the expected theoretical value for the ratio of charged to neutral D mesons which is approximately equal to $\frac{1}{3}$ and is the same for the proton and pion induced interactions². The big difference between the D^+ and D^0 production results from the fact that D mesons can be produced either directly or through feed-down from D^* decays. The prediction for the ratio is obtained by taking into account the well known branching ratios for the decays of D^* into D mesons.

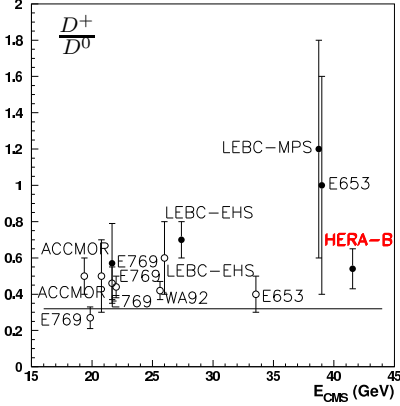


Figure 5: Ratio between D^+ and D^0 production cross sections. The line shows theoretical expectation.

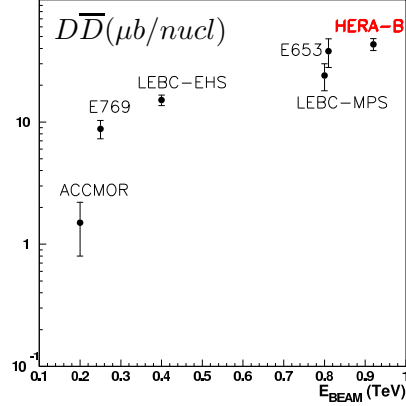


Figure 6: Comparison of our $D\bar{D}$ cross section with the results from previous experiments.

Our result on $D\bar{D}$ cross section is shown in Fig. 6. It is compatible with previous data and has smaller experimental uncertainty in comparison with the experiments at nearby proton beam energies.

5 Preliminary results. The Di-lepton Data

5.1 The Di-lepton invariant mass spectra

The $\mu^+\mu^-$ and e^+e^- invariant mass spectra are shown in Fig. 7 and Fig. 8 respectively. Clear J/ψ and $\psi(2S)$ resonance peaks are visible. Lower mass particle decays of ρ , ω , ϕ into l^+l^- pair are also seen.

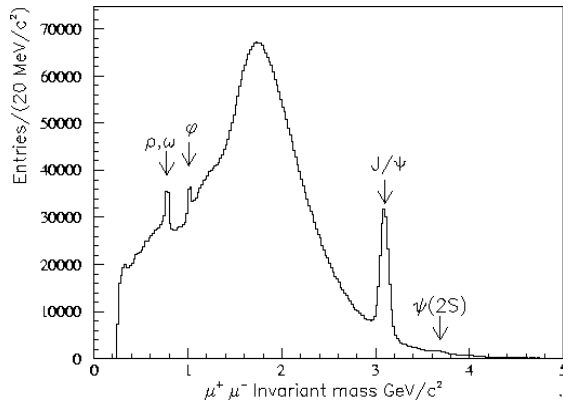


Figure 7: $\mu^+\mu^-$ invariant mass spectrum. Di-lepton trigger.

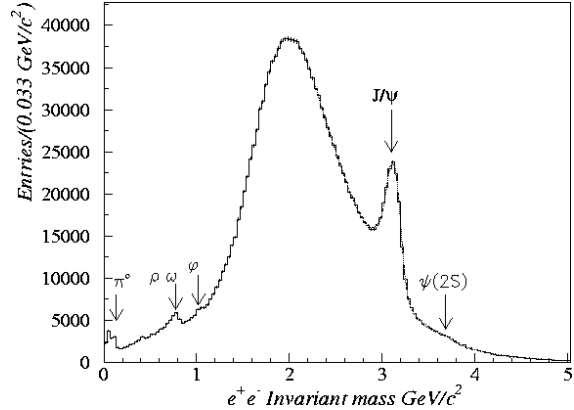


Figure 8: e^+e^- invariant mass spectrum. Di-lepton trigger.

5.2 J/ψ Differential Distributions

The huge sample of J/ψ decays accumulated in 2002/2003 and the large acceptance covered by the HERA-B spectrometer provide a broad coverage in p_T , up to 4.8 GeV. The differential distribution for J/ψ as a function of transverse momentum is shown in Fig. 9. Superimposed on the plot is a fit to the parameterization function:

$$\frac{d\sigma}{dp_T^2} = A \cdot \left[1 + \left(\frac{35 \cdot \pi \cdot p_T}{256 \cdot \langle p_T \rangle} \right)^2 \right]^{-6}$$

Our results on the average transverse momentum as well as the results^{3,4} from E771 and E789 experiments are shown in Table 3. The results obtained in electron and muon channel are compatible with each other for each target material. The HERA-B measurement confirms the trend of increasing average p_T with increasing atomic number and energy in the center of mass.

The differential distribution of J/ψ versus Feynman x_F is plotted in Fig. 10. The points and errors are shown along with a fit to the parameterization function:

$$\frac{d\sigma}{dx_F} = A \cdot (1 - |x_F|)^C$$

The HERA-B differs from all other proton-nucleus collision experiments by its large acceptance in the negative x_F region. Our measurement for exponential parameter and the results^{3,4,5} from previous experiments are shown in Table 4. Due to the ongoing acceptance estimations for different running periods, at the moment only a range for the slope is quoted.

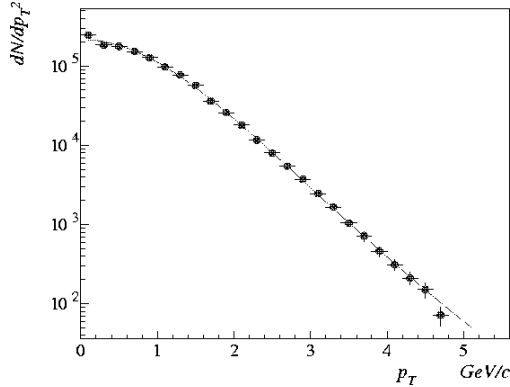


Figure 9: J/ψ differential distribution versus p_T .

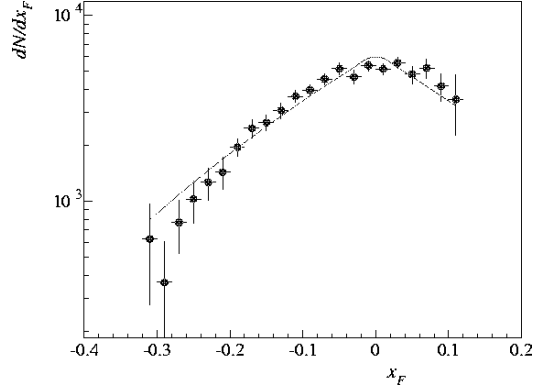


Figure 10: J/ψ differential distribution versus x_F .

Table 3: The HERA-B results on the average transverse momentum for J/ψ . Comparison with data from E771 and E789 experiments.

Experiment	Beam Energy	Target	p_T Range	$\langle p_T \rangle (e^+e^-)$	$\langle p_T \rangle (\mu^+\mu^-)$
HERA-B	920 GeV	C	$p_T < 4.8$ GeV	$1.22 \pm 0.01_{stat}$	$1.22 \pm 0.01_{stat}$
HERA-B	920 GeV	W	$p_T < 4.8$ GeV	$1.29 \pm 0.01_{stat}$	$1.30 \pm 0.01_{stat}$
E771	800 GeV	Si	$p_T < 3.5$ GeV		1.20 ± 0.01
E789	800 GeV	Au	$p_T < 2.6$ GeV		1.29 ± 0.009

Table 4: The HERA-B results on the exponential parameter for J/ψ distribution in x_F . Comparison with data from E771 and E789 experiments.

Experiment	Beam Energy	Target	x_F Range	c
HERA-B	920 GeV	C,W	$-0.35 < x_F < 0.15$	$(5.0 - 6.5) \pm 0.3_{stat}$
E771	800 GeV	Si	$-0.05 < x_F < 0.25$	6.54 ± 0.23
E789	800 GeV	Au	$-0.03 < x_F < 0.13$	4.91 ± 0.18
E789	800 GeV	Cu	$0.30 < x_F < 0.95$	5.21 ± 0.04

5.3 A-Dependence for J/ψ

The suppression of charmonium production in heavy-ion collisions is predicted to be a signature for the formation of the quark-gluon plasma. And it is therefore of particular interest to study these mechanisms in the absence of quark-gluon plasma. In this context the HERA-B presents the new measurement of A-Dependence for J/ψ .

Nuclear effects are usually considered in a power-law parameterization:

$$\sigma_{pA} = \sigma_{pN} \cdot A^\alpha$$

The parameter α can be determined from measurements with two materials:

$$\alpha = \frac{1}{\log(A_W/A_C)} \cdot \log\left(\frac{N_W}{N_C} \frac{\mathcal{L}_C}{\mathcal{L}_W} \frac{\epsilon_C}{\epsilon_W}\right)$$

where N is the number of reconstructed J/ψ 's, L is the integrated luminosity, ϵ - is the detector and trigger efficiency and the acceptance. To reduce the systematic effects only runs with C and W wires operating simultaneously were used.

A-dependence exhibits strong kinematic dependences with Feynman x_F and transverse momentum p_T of the produced J/ψ . Therefore we plot α as a function of x_F , as shown in Fig. 11. Since the ratio of luminosities is under investigation at the moment, the results were normalized to the E866 data⁶.

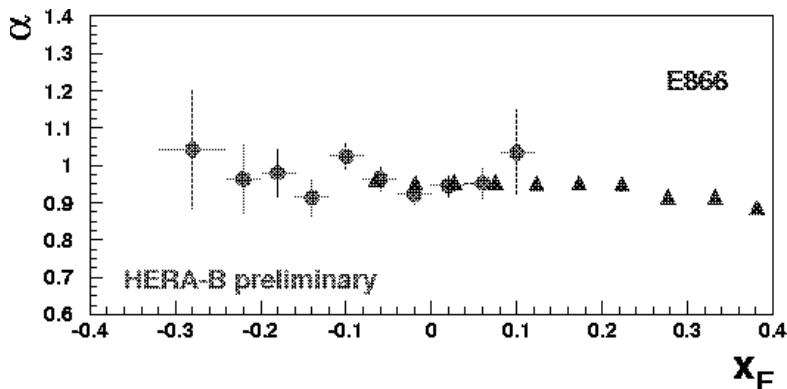


Figure 11: The A-dependence for J/ψ versus x_F . Also shown are the results from E866 experiment.

5.4 Production ratio of $\psi(2S)$ to J/ψ

The production ratio of $\psi(2S)$ to J/ψ is determined according to:

$$R_{\psi(2S)} = \frac{\sigma(\psi(2S))}{\sigma(J/\psi)} = \frac{N(\psi(2S))}{N(J/\psi)} \cdot \frac{Br(J/\psi \rightarrow l^+l^-)}{Br(\psi(2S) \rightarrow l^+l^-)} \cdot \frac{\epsilon(J/\psi)}{\epsilon(\psi(2S))}$$

The electron channel (see Fig. 12) gives $0.13 \pm 0.02_{stat}$ for the $R_{\psi(2S)}$ ratio, which is in good agreement with the result from the muon channel. We also measure the $\psi(2S)$ cross section relative to the J/ψ . The advantage of this method is that detector and trigger efficiencies largely cancel. The value for the J/ψ cross section is based on E771 and E789 measurements^{7,8} and corresponds to $\sigma(J/\psi) = 357 \pm 8_{stat} \pm 27_{sys} nb/nucl$ ⁹. The resulting value for the $\psi(2S)$ cross section is $\sigma(\psi(2S)) = 46 \pm 12_{stat} nb/nucl$ and is shown in Fig. 13 along with the results from previous experiments.

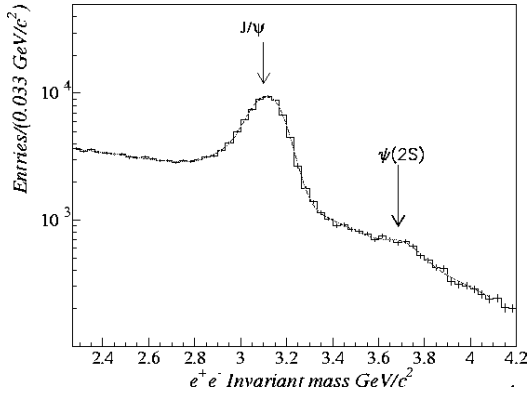


Figure 12: The e^+e^- invariant mass distribution. J/ψ and $\psi(2S)$ resonances are visible.

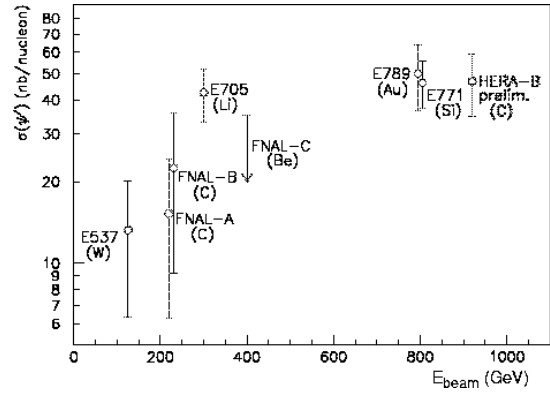


Figure 13: The proton beam energy dependence of the $\psi(2S)$ production cross section.

5.5 Fraction of J/ψ produced via χ_c decays

The production ratio of χ_c to J/ψ can help to discriminate between different theoretical models. The χ_c is reconstructed in the decay $\chi_c \rightarrow J/\psi\gamma \rightarrow l^+l^-\gamma$. Due to the small branching ratio of $\chi_{c0} \rightarrow J/\psi\gamma$, only χ_{c1} and χ_{c2} contribute to the observed χ_c signal. The energy resolution in the HERA-B is insufficient to distinguish χ_{c1} and χ_{c2} states. The fraction of J/ψ produced via radiative χ_c decays is determined from:

$$R_{\chi_c} = \frac{\sum_{i=1}^2 \sigma(\chi_{ci}) \cdot Br(\chi_{ci} \rightarrow J/\psi\gamma)}{\sigma(J/\psi)} = \frac{N(\chi_c)}{N(J/\psi)} \cdot \frac{\epsilon(J/\psi)}{\epsilon(\chi_c) \cdot \epsilon(\gamma)}$$

The published result based on data from an earlier HERA-B run with limited statistics for χ_c is $R_{\chi_c} = 0.32 \pm 0.06_{stat} \pm 0.04_{sys}$ ¹⁰, which is compatible with most of the previous data and the NRQCD prediction.

In the 2002/2003 HERA run, HERA-B collected a χ_c sample which significantly exceeds the statistics obtained by previous experiments. The mass difference distribution $\Delta M = M(l^+l^-\gamma) - M(l^+l^-)$ is shown in Fig. 14. An excess of events with respect to combinatorial background determines the number of χ_c candidates. The same plot, but after background subtraction is shown in Fig. 15. The shape of the background is taken by combining J/ψ and photon candidates from different events. The plot corresponds to 15% of statistics available in muon channel. We expect about 15,000 χ_c for the full data set combined from electron and muon samples. The preliminary result for R_{χ_c} from the 2002/2003 data is $0.21 \pm 0.05_{stat}$.

6 Summary

HERA-B has finished data-taking and now focuses on analysis of large accumulated data samples: 150 million of events with di-lepton trigger and 210 million of events with minimum bias

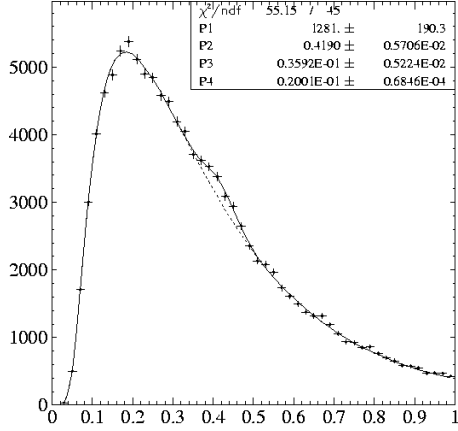


Figure 14: The $\Delta M = M(l^+l^-\gamma) - M(l^+l^-)$ distribution.

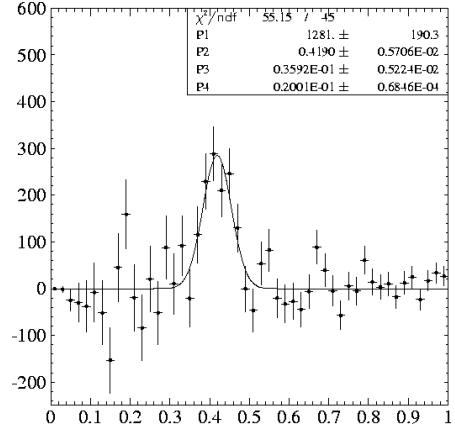


Figure 15: The χ_c signal after background subtraction.

trigger. These data were obtained on a variety of nuclear targets. About 300,000 J/ψ 's decaying into electron and muon pairs were reconstructed in the di-lepton sample. HERA-B features broad coverage in p_T and explores the negative x_F region for the first time. Differential distributions for J/ψ as functions of p_T and x_F are shown. New data on J/ψ suppression are presented. Results on the production ratios of $\psi(2S)$ to J/ψ and χ_c to J/ψ are also shown. Clear signals of D^+ , D^0 and D^{*+} mesons were obtained in the minimum bias data. Results on D^+ and D^0 production cross sections and the D^+ to D^0 ratio are discussed.

Lots of physics analyses are ongoing and we are looking forward to new results.

References

1. M. T. Nunez Pardo de Vera, *Nucl. Phys. Proc. Suppl.* **120**:166-172 (2003).
2. S. Frixione, M. L. Mangano, P. Nason, G. Ridolfi, *Adv. Ser. Direct. High Energy Phys.* **15** 609-706 (1998).
3. T. Alexopoulos *et al*, *Phys. Rev. D* **55**, 3927 (1997).
4. M.H. Schub *et al*, *Phys. Rev. D* **52**, 1307 (1995).
5. M.S. Kowitt *et al*, *Phys. Rev. Lett.* **72**, 1318 (1994).
6. M.J. Leich *et al*, *Phys. Rev. Lett.* **84**, 3256 (2000).
7. T. Alexopoulos *et al*, *Phys. Rev. Lett.* **82**, 41 (1999).
8. D. M. Jansen *et al*, *Phys. Rev. Lett.* **74**, 3118 (1995).
9. I. Abt *et al*, *Eur. Phys. J. C* **26**, 345 (2003).
10. I. Abt *et al*, *Phys. Lett. B* **561**, 61 (2003).